Research Square

Preprints are preliminary reports that have not undergone peer review.
They should not be considered conclusive, used to inform clinical practice,
or referenced by the media as validated information.

Quantitative Resting-State Functional Magnetic Resonance Imaging Reveals White Matter Network Reorganization in Older Adults With White Matter Hyperintensities

Renjie Ma
Xinghua People's Hospital Affiliated to Yangzhou University
Jiajun Li
Yangzhou University
Yuting Zhang
Yangzhou Clinical Medical College of Xuzhou Medical University
Shumin Wei
Xinghua People's Hospital Affiliated to Yangzhou University
Yu Wang
Xinghua People's Hospital Affiliated to Yangzhou University
Chun Cao
Xinghua People's Hospital Affiliated to Yangzhou University
Qingqing Fang
Xinghua People's Hospital Affiliated to Yangzhou University
Tingjin Jin
Xinghua People's Hospital Affiliated to Yangzhou University
Yi Yang
yivictor6@163.com

Xinghua People's Hospital Affiliated to Yangzhou University

Research Article

Keywords: white matter hyperintensities, cerebral small vessel disease, white matter BOLD, resting-state fMRI, functional connectivity, graph theory, topological organization, cognitive impairment

Posted Date: November 25th, 2026

DOI: https://doi.org/10.21203/rs.3.rs-11350070/v1

License: This work is licensed under a Creative Commons Attribution 4.0 International License.
Read Full License

Additional Declarations: No competing interests reported.

Abstract

Background/Objectives:

White matter hyperintensities (WMH) are important imaging markers of cerebral small vessel disease in older adults and are closely associated with cognitive decline. However, WMH burden alone cannot fully explain interindividual differences in cognitive impairment. This study constructed white matter resting-state functional networks based on the multimodal white matter atlas (MWMA) and investigated WMH-related alterations in network topology and their associations with cognitive function.

Methods

This single-center cross-sectional study included 171 older adults, comprising 50 participants with absent or mild white matter hyperintensities and 121 participants with moderate-to-severe white matter hyperintensities. All participants underwent three-dimensional T1-weighted imaging, T2-FLAIR imaging, and resting-state BOLD-fMRI. WMH grading and segmentation were performed using T2-FLAIR images. White matter network nodes were defined using the MWMA atlas, and 173 cerebral white matter regions of interest were retained. Individual 173 × 173 white matter functional connectivity matrices were constructed. Graph-theoretical metrics were calculated across a sparsity range of 0.05–0.50, and area under the curve values were used for statistical analysis. Group differences were assessed using general linear models adjusted for age, sex, years of education, and mean framewise displacement. Exploratory partial correlation analyses were performed in participants with complete cognitive data.

Results

Both groups retained small-world organization. Compared with controls, the WMH group showed increased aγ and aσ, whereas aEglob, aEloc, and aLp did not differ significantly. The WMH group also showed increased DMN-SMN inter-module connectivity, without significant intra-module differences. Nodal abnormalities were spatially heterogeneous: increased aBc was mainly located in WMH-affected regions, whereas abnormal aDc and aNe were more often distributed in normal-appearing white matter. Several abnormal nodal metrics were associated with TMT-A, TMT-B, and MoCA performance.

Conclusions

Moderate-to-severe WMH is associated with white matter functional network reorganization rather than complete topological breakdown. These alterations may contribute to WMH-related cognitive decline, particularly impairments in processing speed and executive function.

Introduction

White matter hyperintensities (WMH) are common findings on brain MRI in older adults and are important imaging markers of cerebral small vessel disease(1, 2). Previous studies have shown that increased WMH burden is closely associated with cognitive decline, especially impairments in executive function, information processing speed, and attentional control(3, 4). However, clinical practice and neuroimaging studies also indicate that WMH burden does not always correspond closely to the severity of cognitive impairment. This suggests that lesion volume alone is insufficient to explain the effect of WMH on cognitive function(5, 6). Therefore, the imaging mechanisms of WMH-related cognitive impairment need to be further clarified from the perspective of altered brain functional organization.

Resting-state functional magnetic resonance imaging (rs-fMRI) evaluates functional connectivity between brain regions by analyzing spontaneous low-frequency fluctuations in blood oxygen level-dependent signals. It provides an important tool for investigating WMH-related abnormalities in brain function(7). Previous rs-fMRI studies of WMH have mainly used gray matter or cortical regions as network nodes. These studies have focused on the effects of WMH on remote cortical functional networks and interregional gray matter functional connectivity(8–10). Such studies have improved the understanding of remote functional abnormalities related to WMH. However, because WMH primarily occur in white matter, functional connectivity analyses based only on gray matter nodes may not directly characterize functional synchronization and network organization within the affected white matter regions.

In traditional rs-fMRI analyses, white matter BOLD signals have often been treated as nuisance signals. As a result, functional information within white matter has received limited attention. In recent years, increasing evidence has shown that white matter BOLD signals are not simply noise. Instead, they may contain functional information related to neural activity, fiber tract architecture, and brain network organization(11, 12). Peer et al. found that resting-state white matter BOLD signals can form symmetric and modular white matter functional networks(13). Huang et al. further showed that spontaneous BOLD signals within white matter exhibit functional connectivity patterns corresponding to fiber tract organization(14). More recently, the multimodal white matter atlas (MWMA) has provided a standardized parcellation framework for white matter functional connectivity analysis(15). This makes it possible to systematically investigate the effects of WMH on white matter functional network organization.

Based on this background, the present study constructed white matter resting-state functional connectivity networks in older adults using the MWMA atlas. First, this study evaluated whether white matter functional networks exhibited small-world properties. Second, global topology, modular connectivity, and nodal topology were compared between individuals with different WMH burdens. Finally, the associations between abnormal white matter network metrics and cognitive performance were explored in participants with complete cognitive data. This study aimed to provide new imaging evidence for understanding WMH-related cognitive decline from the perspective of white matter functional organization.

Materials and Methods

Participants

This single-center cross-sectional observational study consecutively recruited older participants who visited or were examined at the Department of Neurology of the study center between January 2025 and April 2026. The inclusion criteria for the WMH group were as follows: (1) age ≥ 60 years; (2) brain MRI showing Fazekas grade 2–3 WMH; and (3) ability to complete rs-fMRI. The exclusion criteria were as follows: (1) a history of definite neurological diseases, such as stroke, traumatic brain injury, or brain tumor; (2) Parkinson disease, Alzheimer disease, or other diagnosed neurodegenerative diseases; (3) severe psychiatric disorders; and (4) poor MRI image quality or excessive head motion. Excessive head motion was defined as a maximum translation of more than 2.0 mm in any direction or a maximum rotation of more than 2.0° around any axis.

After screening, 121 participants with Fazekas grade 2–3 WMH were included in the WMH group. During the same period, 50 older participants with Fazekas grade 0–1 WMH were recruited from the same center as the control group. These participants were matched with the WMH group for age, sex, and years of education. The remaining inclusion and exclusion criteria for the control group were the same as those for the WMH group. Among all participants, 31 controls and 56 participants with WMH completed the Montreal Cognitive Assessment (MoCA), Trail Making Test A (TMT-A), and Trail Making Test B (TMT-B) within 24 h before MRI scanning. The study protocol was approved by the ethics committee of the study center (approval No.2023js011), and all participants provided written informed consent.

MRI Acquisition

All participants underwent brain MRI using a 3.0-T MRI scanner (Discovery MR750, GE Healthcare, Milwaukee, WI, USA) with a 24-channel phased-array head coil. The MRI protocol included high-resolution three-dimensional T1-weighted imaging, T2-weighted fluid-attenuated inversion recovery imaging (T2-FLAIR), and resting-state BOLD-fMRI. T2-FLAIR images were used for WMH grading and segmentation. Three-dimensional T1-weighted images were used for anatomical registration, and resting-state BOLD-fMRI data were used to construct white matter functional connectivity networks.

High-resolution three-dimensional T1-weighted images were acquired using a brain volume imaging sequence with the following parameters: repetition time (TR) = 7.7 ms, echo time (TE) = 3.1 ms, inversion time (TI) = 450 ms, flip angle (FA) = 12°, field of view (FOV) = 240 mm × 240 mm, matrix size = 256 × 256, and voxel size = 0.9 mm × 0.9 mm × 1.2 mm. T2-FLAIR images were acquired using a fast spin-echo sequence with the following parameters: TR = 9023 ms, TE = 145 ms, TI = 2274 ms, FA = 111°, FOV = 240 mm × 240 mm, matrix size = 256 × 256, slice thickness = 5.0 mm, and no interslice gap. Resting-state BOLD-fMRI data were acquired using a gradient-echo single-shot echo-planar imaging sequence with the following parameters: TR = 2100 ms, TE = 30 ms, FA = 90°, FOV = 224 mm × 224 mm, matrix size = 64 × 64, slice thickness = 3.6 mm, and interslice gap = 0.7 mm. A total of 33 axial slices were acquired in an

interleaved order, and the scanning time was 8 min 24 s. During scanning, participants were instructed to keep their eyes closed, remain awake, and minimize head motion.

WMH Grading and Segmentation

WMH severity was assessed on T2-FLAIR images using the Fazekas visual rating scale(16). Fazekas grade 0 was defined as no visible WMH, grade 1 as punctate WMH, grade 2 as early confluent WMH, and grade 3 as large confluent WMH. In this study, participants with Fazekas grades 0–1 were defined as having absent or mild WMH burden and were assigned to the control group. Participants with Fazekas grades 2–3 were defined as having moderate to severe WMH burden and were assigned to the WMH group.

WMH segmentation was performed using T2-FLAIR images. First, each T2-FLAIR image was rigidly registered to the corresponding T1-weighted structural image. WMH lesions were then automatically segmented using the lesion prediction algorithm in the Lesion Segmentation Toolbox (LST, version 3.0.0). The resulting WMH probability maps were binarized using a threshold of 0.5. All WMH segmentation results underwent visual quality control, and manual correction was performed when necessary.

Resting-State fMRI Preprocessing

White matter rs-fMRI data were preprocessed using DPABI V8.2 and MATLAB scripts released by Peer et al.(13). The preprocessing procedure was as follows. First, raw DICOM images were converted into NIfTI format, and the first 10 volumes were removed to reduce the effects of magnetic field instability and participant adaptation on the BOLD signal. Slice timing correction and head motion correction were then performed. All functional images were realigned to the mean functional image. Participants were excluded if the maximum translation exceeded 2.0 mm in any direction or if the maximum rotation exceeded 2.0° around any axis. Framewise displacement (FD) was further calculated to evaluate transient head motion. Volumes with FD > 0.5 mm were defined as motion outliers and were included as nuisance regressors in the subsequent regression model.

For each participant, the T1-weighted structural image was segmented into gray matter, white matter, and cerebrospinal fluid probability maps. Functional images were co-registered to the individual T1-weighted structural image. Individual white matter, gray matter, and cerebrospinal fluid masks were generated based on tissue segmentation results. To reduce the effects of head motion and non-neuronal signals on functional connectivity estimation, nuisance signals were removed using multiple linear regression. The nuisance regressors included 24 head motion parameters, consisting of the six rigid-body motion parameters, their values from the previous time point, and the squares of these terms. Motion outliers and the mean cerebrospinal fluid signal were also included as covariates. Because this

study focused on white matter BOLD signals, the mean white matter signal and global signal were not regressed out to avoid removing the signal of interest.

To minimize contamination of white matter BOLD signals by gray matter signals, a tissue-specific smoothing strategy was applied. Based on individual tissue segmentation results, white matter and gray matter voxels were separately defined using a tissue probability threshold of 0.5. Functional images containing only white matter voxels and those containing only gray matter voxels were then generated. The two tissue-specific functional images were separately smoothed with a 4-mm full width at half maximum isotropic Gaussian kernel and were then recombined. This procedure reduced the risk of gray matter signal spreading into white matter regions during conventional whole-brain smoothing. After smoothing, functional images were normalized to Montreal Neurological Institute space using DARTEL and resampled to a voxel size of 3 × 3 × 3 mm3. Linear trends were removed, and temporal band-pass filtering was performed at 0.01–0.15 Hz to reduce the effects of low-frequency drift and high-frequency physiological noise on resting-state BOLD signals.

White Matter Functional Network Construction

White matter functional network nodes were defined using the MWMA(15). The MWMA contains 200 white matter regions of interest (ROIs). To focus on white matter functional networks within the cerebral hemispheres and to reduce the potential influence of signal differences from the cerebellum and brainstem on network topology, ROIs related to the cerebellum and brainstem were removed. A total of 173 cerebral white matter ROIs were finally retained as network nodes.

For each participant, the mean preprocessed BOLD time series was extracted from each white matter ROI. Pearson correlation analysis was then performed between the mean time series of each pair of white matter ROIs, resulting in an individual 173 × 173 white matter functional connectivity matrix. Correlation coefficients were converted to z values using Fisher r-to-z transformation to improve normality. These z-transformed matrices were used for subsequent functional connectivity and graph-theoretical analyses. To reduce the influence of negative correlations on the interpretation of network topology, only positive connections were retained for graph-theoretical analysis, and negative values were set to 0. All functional connectivity matrices were analyzed for graph-theoretical topological properties using GRETNA 2.0.0.

Topological and Modular Analyses of White Matter Functional Networks

The workflow for white matter functional network construction and topological analysis is shown in Fig. 2A. Based on the individual 173 × 173 white matter functional connectivity matrices, this study first analyzed global network topological properties. According to previous graph-theoretical network analysis methods(17, 18), each individual white matter functional connectivity matrix was converted into a binary matrix across a range of sparsity thresholds. Network sparsity was defined as the ratio of

retained edges to the maximum possible number of edges in the network. To reduce the influence of a single threshold selection on network topology, a sparsity range of 0.05–0.50 was used with an interval of 0.01. At each sparsity threshold, individual-level network topological metrics were calculated. The area under the curve (AUC) across the whole sparsity range was then computed for each metric and used as a stable topological measure for subsequent statistical analyses.

The global topological metrics included normalized clustering coefficient (γ), normalized characteristic path length (λ), small-worldness (σ), clustering coefficient (Cp), characteristic path length (Lp), global efficiency (Eglob), and local efficiency (Eloc). At the nodal level, the same sparsity threshold range and AUC strategy were used to calculate nodal topological metrics. These metrics were used to identify the spatial distribution of WMH-related abnormalities in white matter networks. The nodal metrics included nodal betweenness centrality (Bc), nodal degree centrality (Dc), and nodal efficiency (Ne).

At the modular level, the 173 white matter ROIs were divided into five white matter functional modules according to the predefined functional network assignments of the MWMA atlas. These modules included the default mode network (DMN), frontoparietal network (FPN), sensorimotor network (SMN), auditory network (AN), and visual network (VN). To assess the effects of WMH on within-system and between-system coupling across white matter functional systems, both intra-module and inter-module functional connectivity strengths were calculated. Intra-module functional connectivity was defined as the mean Fisher z-transformed functional connectivity value across all pairs of ROIs within the same module. Inter-module functional connectivity was defined as the mean Fisher z-transformed functional connectivity value across all ROI pairs between two different modules. For the five functional modules, five intra-module connectivity metrics and ten inter-module connectivity metrics were calculated.

Statistical Analysis

Statistical analyses were performed using MATLAB R2022b and Python 3.10. Continuous variables were first assessed for normality using the Shapiro-Wilk test. Normally distributed continuous variables are presented as mean ± standard deviation, whereas non-normally distributed variables are presented as median and interquartile range. Categorical variables are presented as numbers and percentages. Between-group differences in demographic and clinical variables were assessed using independent-sample t tests, Mann-Whitney U tests, chi-square tests, or Fisher exact tests, as appropriate.

The small-world organization of white matter functional networks was evaluated according to the criteria of $\gamma > 1$, $\lambda \approx 1$, and $\sigma > 1$. Group differences in global topological properties, nodal topological properties, and intra-module and inter-module functional connectivity strength were analyzed using general linear models. Group was entered as the independent variable, and age, sex, years of education, and mean FD were included as covariates. False discovery rate (FDR) correction was applied for multiple comparisons. After FDR correction, $q < 0.05$ was considered statistically significant.

In participants with complete cognitive data, partial correlation analyses were further performed to assess the associations between abnormal white matter network measures and cognitive performance.

Age, sex, years of education, and mean FD were included as covariates in these analyses. All statistical tests were two-sided. The cognitive correlation analyses were considered exploratory and were not corrected for multiple comparisons. For these exploratory analyses, an uncorrected $p < 0.05$ was considered statistically significant.

Results

Participant Characteristics

A total of 171 older participants were included, comprising 50 controls and 121 participants with WMH. The clinical and cognitive characteristics of the participants are summarized in Table 1. The two groups were comparable in age, sex, years of education, body mass index, diabetes mellitus, hyperlipidemia, smoking status, diastolic blood pressure, and mean FD. Compared with controls, the WMH group had a higher prevalence of hypertension, higher systolic blood pressure, higher Fazekas grades, and larger WMH volume. The WMH group also showed lower MoCA scores and longer TMT-A, TMT-B, and TMT B-A completion times. Figure 1 shows the spatial distribution of WMH in the two groups. Controls mainly showed no visible lesions or only a few punctate WMH, whereas the WMH group showed more extensive and confluent lesions, mainly involving the periventricular and deep white matter regions.

Table 1
Clinical and Cognitive Characteristics of the Participants

Age, years	**Controlgroup (n = 50)**	**WMHgroup (n = 121)**	***p***
	68.2 ± 5.7	**69.4 ± 6.3**	**0.25**
Male sex, n(%)	24(48.0)	63(52.1)	0.63
Years of education	9.0(6.0–12.0)	8.0(6.0–12.0)	0.39
BMI, kg/m^2	24.1 ± 3.0	24.8 ± 3.2	0.19
Hypertension, n(%)	21(42.0)	79(65.3)	**0.006**
Diabetes mellitus, n(%)	9(18.0)	34(28.1)	0.17
Hyperlipidemia, n(%)	16(32.0)	47(38.8)	0.40
Current or former smoking n(%)	15(30.0)	41(33.9)	0.62
Systolic blood pressure, mmHg	132.4 ± 14.8	141.0 ± 17.5	**0.003**
Diastolic blood pressure, mmHg	78.1 ± 9.2	80.2 ± 10.1	0.21
Fazekas grade, 0/1/2/3	18/32/0/0	0/0/76/45	**< 0.001**
WMH volume, mL	1.3(0.5–2.8)	18.7(10.4–34.6)	**< 0.001**
Mean framewise displacement, mm	0.13(0.09–0.19)	0.15(0.10–0.22)	0.18
Participants with cognitive data, n	31	56	
MoCA score	24.00 ± 3.35	20.77 ± 3.92	**< 0.001**
TMT A, s	41.00(31.50–61.00)	83.00(61.00-106.00)	**< 0.001**
TMT B, s	103.00(83.50-149.50)	201.00(155.00-278.75)	**< 0.001**
TMT B-A, s	66.00(44.00–95.00)	102.00(78.25-185.75)	**< 0.001**

Note. Data are presented as mean ± standard deviation, median (interquartile range), or number (percentage), as appropriate. Between-group comparisons were performed using independent-sample t tests, Mann–Whitney U tests, chi-square tests, or Fisher exact tests, as appropriate. Participants in the control group had absent or mild WMH burden, defined as Fazekas grades 0–1, whereas participants in the WMH group had moderate-to-severe WMH burden, defined as Fazekas grades 2–3.

Abbreviations: BMI, body mass index; DBP, diastolic blood pressure; FD, framewise displacement; HC, control group; MoCA, Montreal Cognitive Assessment; SBP, systolic blood pressure; TMT A, Trail Making

Test Part A; TMT B, Trail Making Test Part B; TMT B-A, difference between TMT B and TMT A completion times; WMH, white matter hyperintensities.

Small-World Organization and Altered Global Topology of White Matter Functional Networks

Across the predefined sparsity range, white matter functional networks in both groups showed typical small-world organization. In both the control and WMH groups, γ was greater than 1, λ was close to 1, and σ was greater than 1 (Fig. 2B-D), indicating preserved small-world organization. Further comparison of the AUC values for global topological metrics showed that aγ and aσ were significantly higher in the WMH group than in the control group, and both differences survived FDR correction. No significant between-group differences were observed in the remaining global topological metrics (Fig. 3A and Supplementary Table 1).

Altered Intra-Module and Inter-Module Connectivity in White Matter Functional Networks

No significant between-group differences were observed in intra-module functional connectivity within the DMN, FPN, SMN, AN, or VN (Fig. 3B and Supplementary Table 2). Inter-module functional connectivity was further compared across the five functional modules. DMN-SMN inter-module connectivity was significantly higher in the WMH group than in the control group, and this difference survived FDR correction. SMN-AN and AN-VN inter-module connectivity showed between-group differences at the uncorrected level, but these differences did not survive FDR correction. No significant group differences were observed in the remaining inter-module connections (Fig. 3C and Supplementary Table 3).

Altered Nodal Topological Properties and Their Spatial Relationship with WMH Distribution

Further comparison of nodal topological properties showed focal abnormalities in several white matter nodes in the WMH group (Supplementary Table 4). For nodal betweenness centrality, five nodes showed significantly increased aBc in the WMH group (Fig. 4A). Among these nodes, three belonged to the DMN and two belonged to the SMN. These nodes mainly overlapped with regions affected by WMH lesions (Fig. 4B). For nodal degree centrality, seven nodes showed abnormalities in the WMH group. Six nodes showed increased aDc and involved the DMN, SMN, VN, and AN, whereas one SMN node showed decreased aDc (Fig. 4C). These abnormal aDc nodes were mainly located in normal-appearing white matter regions (Fig. 4D). For nodal efficiency, only one AN node showed increased aNe in the WMH group (Fig. 4E), and this node was also mainly located in normal-appearing white matter (Fig. 4F). Overall, WMH-related nodal topological abnormalities showed spatial heterogeneity, characterized by increased aBc in DMN and SMN nodes overlapping with WMH-affected regions, together with altered aDc and aNe in several nodes located in normal-appearing white matter.

Exploratory Associations Between Abnormal White Matter Network Measures and Cognitive Performance

Partial correlation analyses showed that only several nodal topological metrics were associated with cognitive performance at the uncorrected level (Fig. 5 and Supplementary Table 5). Among these findings, abnormal aDc showed the most consistent associations with TMT performance. Higher aDc in MWMA 89 and MWMA 39 was associated with longer TMT-A completion time, and higher aDc in MWMA 89 was also associated with longer TMT-B completion time. In contrast, aDc in MWMA 191 was negatively associated with TMT-A completion time. In addition, higher aBc in MWMA 66 and MWMA 26 was associated with longer TMT-B and TMT-A completion times, respectively. For global cognitive function, aDc in MWMA 39 was negatively associated with MoCA score, whereas aDc in MWMA 179 was positively associated with MoCA score.

Discussion

This study constructed white matter rs-fMRI networks in older adults based on the MWMA atlas and systematically investigated WMH-related alterations in white matter functional network topology and their associations with cognitive function. The results showed that white matter functional networks in both the control and WMH groups retained small-world organization, suggesting that white matter BOLD signals can form organized functional network structures. Compared with controls, the WMH group showed increased aγ and aσ, indicating enhanced local clustering and possible network reorganization. Further modular analysis showed increased inter-module functional connectivity between the DMN and SMN in the WMH group, whereas no significant differences were observed in intra-module connectivity. Nodal analysis further revealed spatial heterogeneity in WMH-related topological abnormalities. Nodes with increased aBc were mainly located in regions affected by WMH lesions, while abnormalities in aDc and aNe were more frequently distributed in normal-appearing white matter. Exploratory correlation analyses showed that several abnormal nodal topological metrics were associated with TMT and MoCA performance. These findings suggest that white matter functional network abnormalities may be involved in WMH-related cognitive impairment. Overall, WMH may not only represent focal structural lesions but may also be accompanied by broader reorganization of white matter functional networks. This provides new functional network evidence for understanding WMH-related cognitive decline.

The present study found that white matter functional networks in both the control and WMH groups retained small-world organization. This finding suggests that white matter BOLD signals can form organized functional network structures, even in the presence of moderate to severe WMH. It is also consistent with recent evidence showing that white matter BOLD signals have reproducible functional network organization. Previous studies have shown that white matter functional networks are not random noise. Instead, they can exhibit stable static and dynamic connectivity patterns, and their connectivity strength and dynamic features may change with aging(19). Therefore, this study further demonstrates that white matter node-based functional networks have interpretable topological

organization in older adults with WMH. Notably, the WMH group showed increased aγ and aσ, whereas aEglob, aEloc, and aLp did not differ significantly between groups. This pattern should not be simply interpreted as improved network function. Rather, it may indicate a shift toward stronger local clustering and local segregation in white matter functional networks under the influence of WMH. Previous CSVD studies have also reported alterations in resting-state functional network topology related to small vessel disease. However, the direction of global network changes has not been fully consistent across studies(20, 21). The present findings suggest that WMH does not lead to a complete breakdown of global white matter functional network topology. Instead, the basic network architecture may be partly maintained through increased local clustering. This change may reflect a compensatory response, but it may also represent inefficient reorganization under conditions of reduced information transfer efficiency.

At the modular level, no significant differences were observed in within-module connectivity in the WMH group, whereas connectivity between the DMN and SMN was significantly increased. This finding suggests that the effect of WMH on white matter functional networks is not characterized by a general reduction in synchronization within functional modules. Instead, it may mainly involve abnormally increased coupling between specific functional systems. The DMN is commonly related to internally oriented cognition, memory, and self-referential processing, whereas the SMN is closely involved in sensorimotor integration, motor execution, and somatosensory processing. Increased connectivity between these two systems may indicate reduced functional segregation between higher-order cognitive systems and sensorimotor systems. Previous gray matter functional network studies in CSVD and WMH have also shown that white matter lesion burden can affect connectivity across multiple large-scale networks, especially those involving the SMN, DMN, executive control network, and attention network(22, 23). Recent evidence further suggests that large-scale network connectivity may mediate the associations of white matter lesions with executive function and information processing speed(10). Therefore, the increased connectivity between the DMN and SMN observed in this study may reflect abnormal redistribution of cross-system communication in the context of WMH. This pattern may represent compensatory connectivity enhancement related to disrupted white matter pathways. It may also reflect reduced network differentiation and blurred boundaries between functional systems. Since no significant changes were found in within-module connectivity, a more reasonable interpretation is that WMH mainly affects coordination between white matter functional systems, rather than simply weakening functional coherence within individual modules.

The nodal findings further revealed spatial heterogeneity in WMH-related white matter functional network abnormalities. Increased aBc was mainly observed in regions affected by WMH lesions, whereas abnormalities in aDc and aNe were more frequently distributed in normal-appearing white matter. aBc reflects the extent to which a node participates in shortest communication paths across the network. Therefore, increased aBc in lesion-overlapping white matter regions may indicate that these regions serve as abnormal relay or bottleneck nodes within the white matter functional network. In other words, WMH lesions may not only represent focal structural damage in the traditional sense but may also alter the routing architecture of white matter network communication(24). In contrast, the observation that aDc and aNe abnormalities were more often located in normal-appearing white matter

is particularly important. It suggests that WMH-related functional network abnormalities are not restricted to FLAIR-visible lesions but may extend into white matter that appears normal on conventional imaging(25). Previous diffusion studies have shown that normal-appearing white matter may already show microstructural abnormalities that are associated with poorer cognitive performance(26). A recent habitat analysis study further found that combined diffusion and perfusion parameters can identify white matter regions that may later progress to WMH, and that reduced structural network efficiency related to these regions is associated with cognitive decline(27). Therefore, the aDc and aNe abnormalities in normal-appearing white matter observed in this study may reflect early white matter functional injury or compensatory network reorganization beyond visible WMH lesions. This finding may help explain why WMH volume alone often fails to fully account for the severity of cognitive impairment.

Exploratory correlation analyses showed that several abnormal nodal topological metrics were associated with cognitive performance, with aDc showing the most consistent associations with TMT-A and TMT-B performance. TMT-A mainly reflects information processing speed, visual search, and sustained attention, whereas TMT-B further involves cognitive switching and executive control. Therefore, the present findings suggest that abnormal nodal organization of white matter functional networks may be related to the impairments in processing speed and executive function that are commonly observed in patients with WMH(10). Notably, increased aDc in some nodes was associated with longer TMT completion times. This indicates that a higher number of nodal connections does not necessarily reflect better network function. In the context of WMH, such increased connectedness may represent abnormal rerouting, inefficient compensation, or pathological overcoupling. Previous studies have shown that WMH can affect information processing speed by damaging long-range connections(28). Other evidence indicates that large-scale functional network connectivity may mediate the associations of white matter lesions with executive function and information processing speed(10). Structure-function coupling research also suggests that brain network abnormalities in CSVD are closely related to neurocognitive performance(29). In addition, studies of dynamic functional connectivity have shown that patients with CSVD exhibit abnormal dynamic network connectivity patterns, and these changes are related to cognitive performance(22). In contrast, the associations involving MoCA were fewer and less consistent in direction. This may be related to the limited sensitivity of MoCA as a global screening tool, as well as the smaller sample size for cognitive analyses. Therefore, these correlation results should be regarded as exploratory findings. They suggest that nodal abnormalities in white matter functional networks may contribute to WMH-related cognitive impairment, especially deficits in executive function and information processing speed. Validation in larger samples and longitudinal studies is still needed.

Several limitations should be acknowledged. First, this was a single-center cross-sectional study. Causal relationships among WMH burden, white matter functional network reorganization, and cognitive impairment cannot be determined. Longitudinal follow-up studies are needed to examine whether these network alterations can predict WMH progression and cognitive decline. Second, although age, sex, years of education, and head motion were adjusted for in the statistical analyses, the WMH group had a higher prevalence of hypertension and higher systolic blood pressure than the control group. Residual

confounding related to vascular risk factors cannot be fully excluded. Third, cognitive data were available only in a subset of participants, and the cognitive correlation analyses were not corrected for multiple comparisons. These associations should therefore be interpreted as exploratory findings and require confirmation in larger cohorts. Fourth, white matter BOLD signals may be affected by physiological noise, vascular reactivity, partial volume effects, and gray matter signal contamination. Although tissue-specific smoothing, head motion correction, and nuisance regression were used to reduce these effects, their potential influence cannot be completely excluded. Finally, graph-theoretical results may be influenced by methodological choices, including node definition, sparsity range, binarization, and the handling of negative connections. Future studies should combine weighted networks, dynamic functional connectivity, structural connectivity, perfusion imaging, and diffusion imaging to further clarify the biological basis and clinical significance of WMH-related white matter functional network reorganization.

Conclusions

In conclusion, this study shows that moderate-to-severe WMH is associated with white matter functional network reorganization rather than complete topological breakdown. The main alterations included preserved small-world organization, increased local clustering, enhanced DMN-SMN connectivity, and spatially heterogeneous nodal abnormalities. Notably, abnormal nodal topology was observed not only in WMH-affected regions but also in normal-appearing white matter. Exploratory findings further suggest that these network alterations may be related to cognitive performance, especially processing speed and executive function. These results provide functional network evidence for understanding WMH-related brain dysfunction.

Declarations

Footnote

Reporting Checklist

The authors have completed the STROBE reporting checklist.

Data Sharing Statement

The data generated and analyzed during the current study are not publicly available due to privacy and ethical restrictions but are available from the corresponding author on reasonable request, subject to approval by the institutional ethics committee.

Conflicts of Interest:

All authors have completed the ICMJE uniform disclosure form. The authors have no conflicts of interest to declare.

Funding:

None.

Author Contribution

Conceptualization, R.M. and Y.Y.; methodology, R.M., J.L. and Y.Z.; software, R.M.; validation, S.W., Y.W. and C.C.; formal analysis, R.M.; investigation, R.M., Q.F. and T.J.; resources, Y.Z. and Y.Y.; data curation, R.M. and J.L.; writing-original draft preparation, R.M.; writing-review and editing, J.L., Y.Z. and Y.Y.; visualization, R.M.; supervision, Y.Y.; project administration, Y.Y. All authors have read and agreed to the published version of the manuscript.

Acknowledgments

The authors thank all participants for their involvement in this study.

References

1. Duering M, Biessels GJ, Brodtmann A, Chen C, Cordonnier C, de Leeuw FE et al (2023) Neuroimaging standards for research into small vessel disease-advances since 2013. Lancet Neurol 22(7):602–618. http://doi.org/10.1016/S1474-4422(23)00131-X
2. Wardlaw JM, Smith EE, Biessels GJ, Cordonnier C, Fazekas F, Frayne R et al (2013) Neuroimaging standards for research into small vessel disease and its contribution to ageing and neurodegeneration. Lancet Neurol 12(8):822–838. http://doi.org/10.1016/S1474-4422(13)70124-8
3. Guo W, Shi J (2022) White matter hyperintensities volume and cognition: A meta-analysis. Front Aging Neurosci 14:949763. http://doi.org/10.3389/fnagi.2022.949763
4. Kloppenborg RP, Nederkoorn PJ, Geerlings MI, van den Berg E (2014) Presence and progression of white matter hyperintensities and cognition: a meta-analysis. Neurology 82(23):2127–2138. http://doi.org/10.1212/WNL.0000000000000505
5. Petersen M, Coenen M, DeCarli C, De Luca A, van der Lelij E et al (2024) Alzheimer's Disease Neuroimaging I,. Enhancing cognitive performance prediction by white matter hyperintensity connectivity assessment. Brain. ;147(12):4265-79. http://doi.org/10.1093/brain/awae315
6. Lin YR, Lee WL, Fuh JL (2025) The role of cognitive reserve in white matter hyperintensities: from cognitive aging to Alzheimer's spectrum. Alzheimers Dement (Amst) 17(3):e70167. http://doi.org/10.1002/dad2.70167

7. Fox MD, Raichle ME (2007) Spontaneous fluctuations in brain activity observed with functional magnetic resonance imaging. Nat Rev Neurosci 8(9):700–711. http://doi.org/10.1038/nrn2201
8. Shah C, Srinivasan D, Erus G, Schmitt JE, Agarwal A, Cho ME et al (2021) Changes in brain functional connectivity and cognition related to white matter lesion burden in hypertensive patients from SPRINT. Neuroradiology 63(6):913–924. http://doi.org/10.1007/s00234-020-02614-6
9. Ding JR, Ding X, Hua B, Xiong X, Wen Y, Ding Z et al (2018) Altered connectivity patterns among resting state networks in patients with ischemic white matter lesions. Brain Imaging Behav 12(5):1239–1250. http://doi.org/10.1007/s11682-017-9793-9
10. Chen J, Lu W, Wang Z, Shi M, Shi Z, Shi W (2025) Large-scale functional network connectivity mediate the associations of white matter lesions with executive functions and information processing speed in asymptomatic cerebral small vessels diseases. NeuroImage Clin 46:103773. http://doi.org/10.1016/j.nicl.2025.103773
11. Huang Y, Wei PH, Xu L, Chen D, Yang Y, Song W et al (2023) Intracranial electrophysiological and structural basis of BOLD functional connectivity in human brain white matter. Nat Commun 14(1):3414. http://doi.org/10.1038/s41467-023-39067-3
12. Gore JC, Li M, Gao Y, Wu TL, Schilling KG, Huang Y et al (2019) Functional MRI and resting state connectivity in white matter - a mini-review. Magn Reson Imaging 63:1–11. http://doi.org/10.1016/j.mri.2019.07.017
13. Peer M, Nitzan M, Bick AS, Levin N, Arzy S (2017) Evidence for Functional Networks within the Human Brain's White Matter. J Neurosci 37(27):6394–6407. http://doi.org/10.1523/JNEUROSCI.3872-16.2017
14. Huang Y, Yang Y, Hao L, Hu X, Wang P, Ding Z et al (2020) Detection of functional networks within white matter using independent component analysis. NeuroImage 222:117278. http://doi.org/10.1016/j.neuroimage.2020.117278
15. Zhou J, Li W, Xu S, Biswal BB, Chen H, Li J et al (2026) Multimodal, multifaceted, imaging-based human brain white matter atlas. Sci Bull (Beijing) 71(3):500–504. http://doi.org/10.1016/j.scib.2025.08.021
16. Fazekas F, Chawluk JB, Alavi A, Hurtig HI, Zimmerman RA (1987) MR signal abnormalities at 1.5 T in Alzheimer's dementia and normal aging. AJR Am J Roentgenol 149(2):351–356. http://doi.org/10.2214/ajr.149.2.351
17. Rubinov M, Sporns O (2010) Complex network measures of brain connectivity: uses and interpretations. NeuroImage 52(3):1059–1069. http://doi.org/10.1016/j.neuroimage.2009.10.003
18. Wang J, Wang X, Xia M, Liao X, Evans A, He Y (2015) GRETNA: a graph theoretical network analysis toolbox for imaging connectomics. Front Hum Neurosci 9:386. http://doi.org/10.3389/fnhum.2015.00386
19. LinLi Z, Hu K, Guo Q, Guo S (2025) Static and dynamic connectivity structure of white-matter functional networks across the adult lifespan. Prog Neuropsychopharmacol Biol Psychiatry 136:111252. http://doi.org/10.1016/j.pnpbp.2025.111252

20. Xin H, Wen H, Feng M, Gao Y, Sui C, Zhang N et al (2022) Disrupted topological organization of resting-state functional brain networks in cerebral small vessel disease. Hum Brain Mapp 43(8):2607–2620. http://doi.org/10.1002/hbm.25808
21. Schulz M, Malherbe C, Cheng B, Thomalla G, Schlemm E (2021) Functional connectivity changes in cerebral small vessel disease - a systematic review of the resting-state MRI literature. BMC Med 19(1):103. http://doi.org/10.1186/s12916-021-01962-1
22. Chen F, Chen Q, Zhu Y, Long C, Lu J, Jiang Y et al (2024) Alterations in Dynamic Functional Connectivity in Patients with Cerebral Small Vessel Disease. Transl Stroke Res 15(3):580–590. http://doi.org/10.1007/s12975-023-01148-2
23. Drenth N, Foster-Dingley JC, Bertens AS, Rius Ottenheim N, van der Mast RC, Rombouts S et al (2023) Functional connectivity in older adults-the effect of cerebral small vessel disease. Brain Commun 5(3):fcad126. http://doi.org/10.1093/braincomms/fcad126
24. Chen H, Xu J, Lv W, Hu Z, Ke Z, Qin R et al (2023) Altered morphological connectivity mediated white matter hyperintensity-related cognitive impairment. Brain Res Bull 202:110714. http://doi.org/10.1016/j.brainresbull.2023.110714
25. Silbert LC, Roese NE, Krajbich V, Hurworth J, Lahna D, Schwartz DL et al (2024) White matter hyperintensities and the surrounding normal appearing white matter are associated with water channel disruption in the oldest old. Alzheimer's Dement J Alzheimer's Assoc 20(6):3839–3851. http://doi.org/10.1002/alz.13816
26. Ng YL, Tan CS, Egle M, Gyanwali B, Tozer DJ, Markus HS et al (2023) The association of diffusion tensor MRI measures of normal appearing white matter and cognition. Cereb Circ Cogn Behav 5:100174. http://doi.org/10.1016/j.cccb.2023.100174
27. Han X, Wang Y, Chen Y, Qiu Y, Gu X, Dai Y et al (2024) Predicting white-matter hyperintensity progression and cognitive decline in patients with cerebral small-vessel disease: a magnetic resonance-based habitat analysis. Quant imaging Med Surg 14(9):6621–6634. http://doi.org/10.21037/qims-24-238
28. Lu T, Wang Z, Zhu Y, Wang M, Lu CQ, Ju S (2024) Long-range connections damage in white matter hyperintensities affects information processing speed. Brain Commun 6(1):fcae042. http://doi.org/10.1093/braincomms/fcae042
29. Tay J, During M, van Leijsen EMC, Bergkamp MI, Norris DG, de Leeuw FE et al (2023) Network structure-function coupling and neurocognition in cerebral small vessel disease. NeuroImage Clin 38:103421. http://doi.org/10.1016/j.nicl.2023.103421

Figures

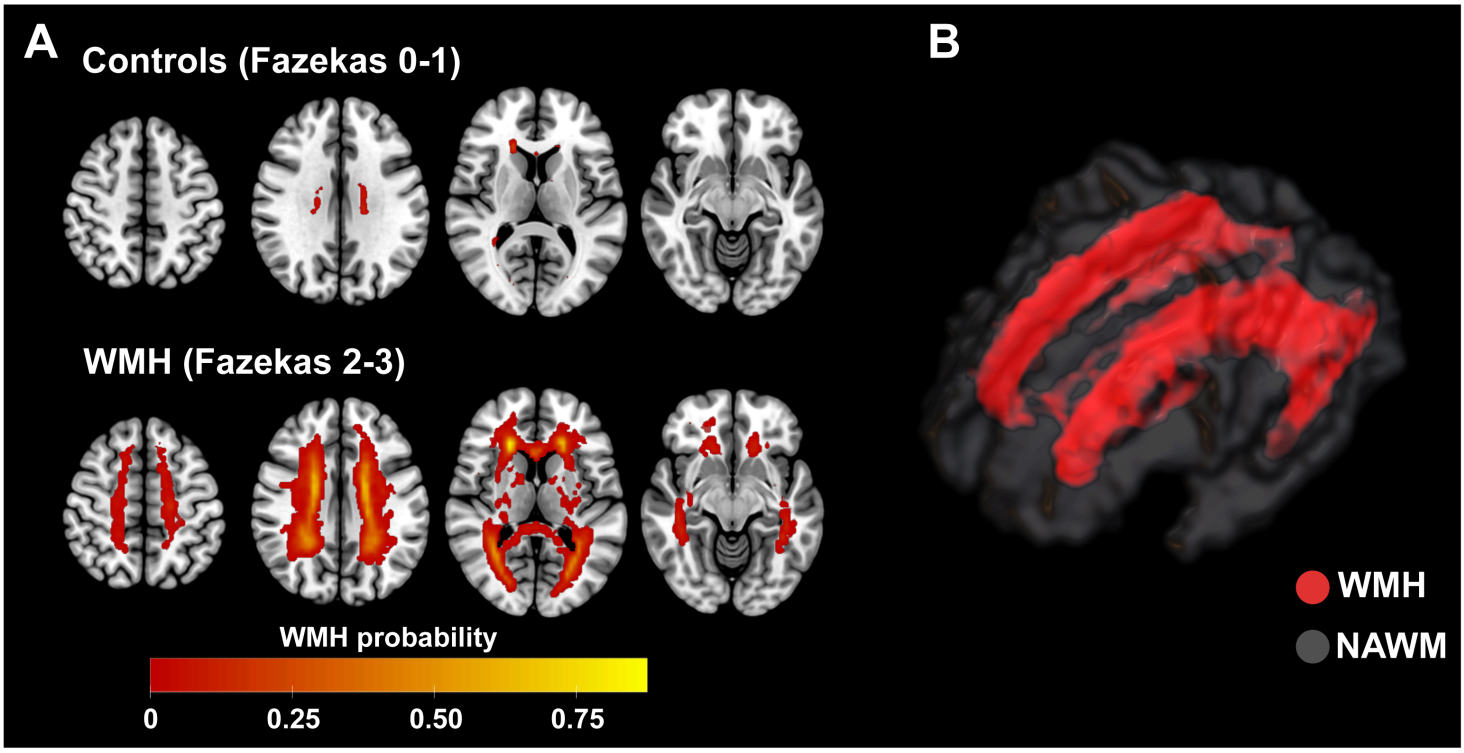

Figure 1

White matter functional network construction and small-world properties.

(A) Workflow of white matter functional network construction and graph-theoretical analysis. (B-D) Changes in λ, γ, and σ across the sparsity range of 0.05-0.50 in the control and WMH groups.

Abbreviations: MWMA, multimodal white matter atlas; ROI, region of interest; WMH, white matter hyperintensities; γ, normalized clustering coefficient; λ, normalized characteristic path length; σ, small-worldness.

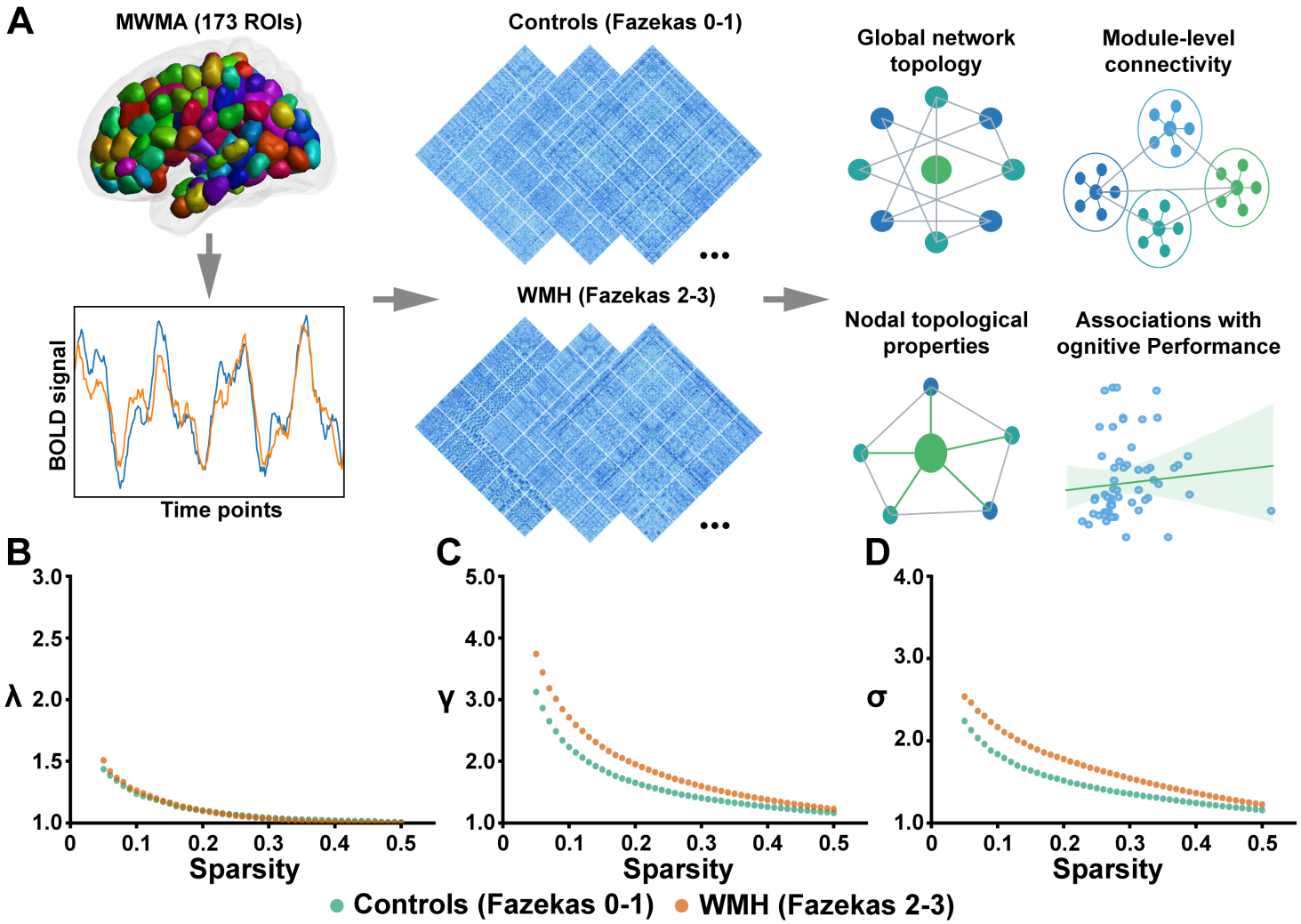

Figure 2

Spatial distribution of white matter hyperintensities.

(A) Group-level WMH probability maps in controls and participants with WMH. (B) Three-dimensional visualization of WMH-affected regions and normal-appearing white matter.

Abbreviations: NAWM, normal-appearing white matter; WMH, white matter hyperintensities.

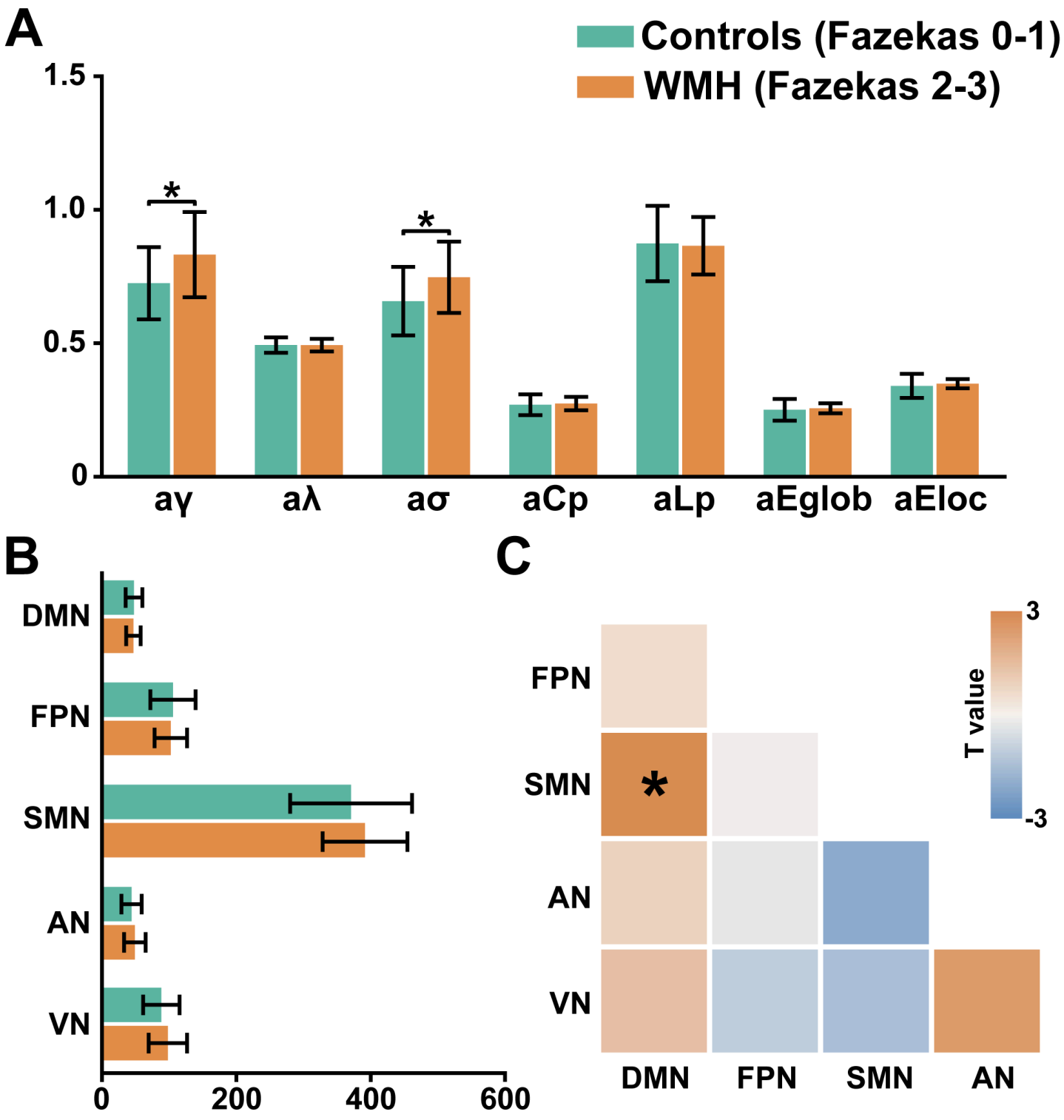

Figure 3

Group differences in global topology and module-level connectivity.

(A) Global topological metrics. (B) Intra-module functional connectivity. (C) Inter-module functional connectivity. The WMH group showed increased aγ, aσ, and DMN-SMN inter-module connectivity.

Abbreviations: AN, auditory network; aCp, area under the curve of clustering coefficient; aEglob, area under the curve of global efficiency; aEloc, area under the curve of local efficiency; aLp, area under the curve of characteristic path length; aγ, area under the curve of normalized clustering coefficient; aλ, area under the curve of normalized characteristic path length; aσ, area under the curve of small-worldness; DMN, default mode network; FPN, frontoparietal network; SMN, sensorimotor network; VN, visual network; WMH, white matter hyperintensities.

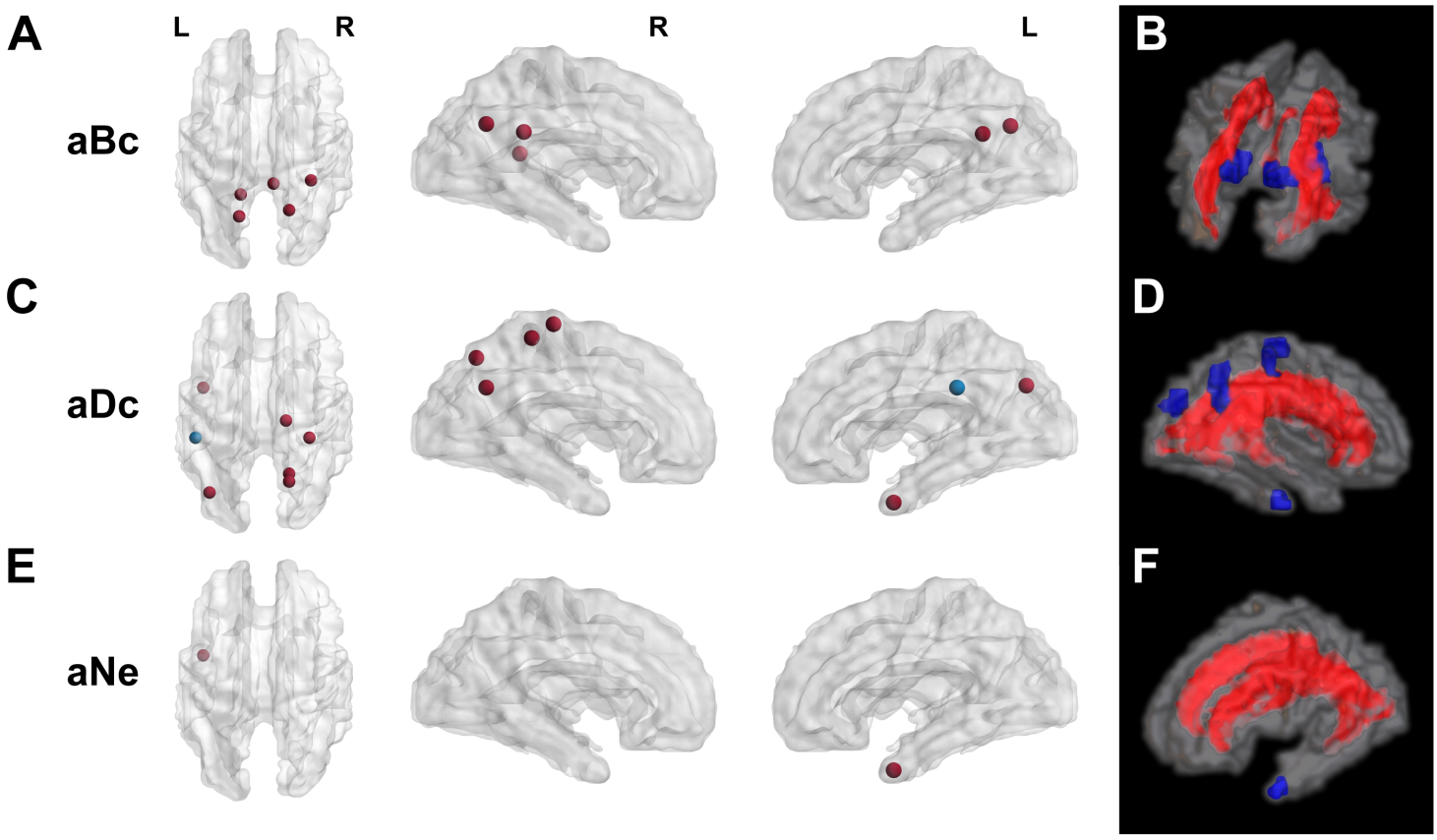

Figure 4

Abnormal nodal topology and its spatial relationship with WMH distribution.

(A, B) Abnormal nodal betweenness centrality and its relationship with WMH distribution. (C, D) Abnormal nodal degree centrality and its relationship with WMH distribution. (E, F) Abnormal nodal efficiency and its relationship with WMH distribution. Red and blue nodes indicate higher and lower values in the WMH group, respectively.

Abbreviations: aBc, area under the curve of nodal betweenness centrality; aDc, area under the curve of nodal degree centrality; aNe, area under the curve of nodal efficiency; NAWM, normal-appearing white matter; WMH, white matter hyperintensities.

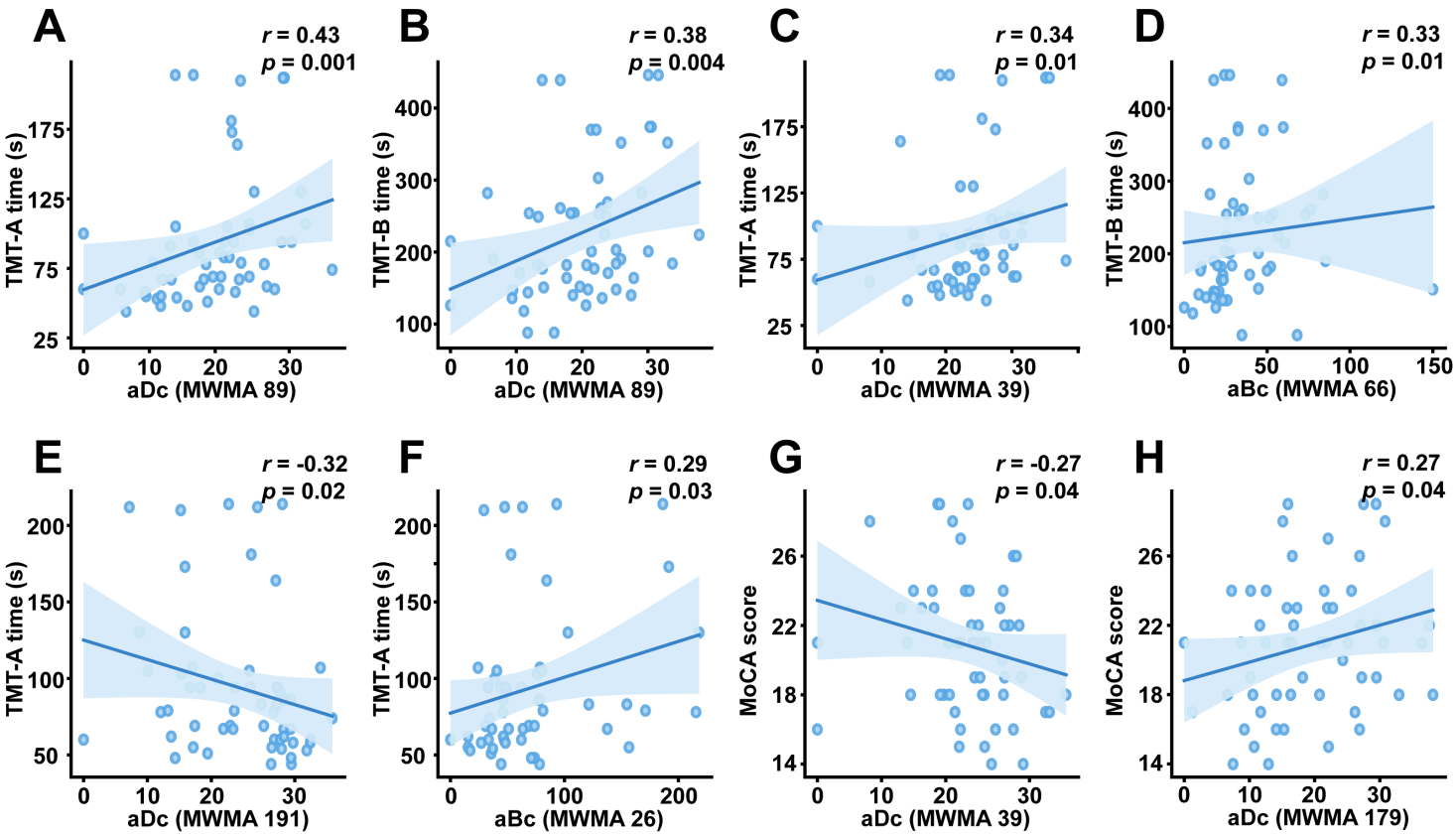

Figure 5

Associations between abnormal nodal metrics and cognitive performance.

(A-H) Exploratory partial correlations between abnormal white matter nodal metrics and cognitive measures after adjustment for age, sex, years of education, and mean framewise displacement. Shaded areas indicate 95% confidence intervals.

Abbreviations: aBc, area under the curve of nodal betweenness centrality; aDc, area under the curve of nodal degree centrality; MoCA, Montreal Cognitive Assessment; MWMA, multimodal white matter atlas; TMT A, Trail Making Test Part A; TMT B, Trail Making Test Part B.

Supplementary Files

This is a list of supplementary files associated with this preprint. Click to download.

- SupplementaryAppendix.docx